Journal of
Materials in Life Sciences

Vol. 5 No. 1 (2026)

Full Paper

Biohydrogen Production by Locally Isolated Purple Non-Sulfur Bacteria: Strain Characterization, OFAT Optimization, and Evaluation of Silver Nanoparticle Effects

Farida Abdulsalam[1], Siti Hajar Mohamad Yusoff[1],Rosalinda Johari[1], Nurliyana Ahmad Zawawi[1], Nurzila Ab Latif[1] and Siti Halimah Hasmoni[1,]

[1]Department of Biosciences, Faculty Science, Universiti Teknologi Malaysia. 81310 UTM Johor Bahru, Johor Darul Ta'zim, Malaysia

Article history
Received
26 March 2026
Revised
21 April 2026
Accepted
28 April 2026
Published online
30 May 2026

*Corresponding author
email: sitihalimah@utm.my.

Abstract

Biohydrogen production by purple non-sulfur bacteria (PNSB) is a promising renewable energy technology; however, low production efficiency, limited characterization of locally isolated strains, and insufficient understanding of the effects of silver nanoparticles hinder its practical application. Therefore, the identification of locally isolatef PNSB strains and optimization of cultivation conditions are necessary to improve hydrogen yield and evaluate the potential of nanoparticle-assisted biohydrogen production. This study investigated biohydrogen production by locally isolated purple non-sulfur bacteria (PNSB), focusing on strain characterization, process optimization, and the effects of silver nanoparticles (AgNPs). Two isolates were obtained and identified: one strain, closely related to *Rhodopseudomonas palustris* (PNSB_P), demonstrated superior hydrogen-producing capability, while the second strain (PNSB_B) showed no detectable production. Growth kinetics revealed that PNSB_P exhibited efficient biomass accumulation despite a lower specific growth rate, indicating effective metabolic allocation toward hydrogen production. Optimization using a one-factor-at-a-time (OFAT) approach showed that the carbon source and growth conditions significantly influenced hydrogen yield ($p < 0.05$), with maltose and strict light–anaerobic conditions yielding the highest yields. In contrast, inoculum size and temperature showed no significant effects ($p > 0.05$) and baseline conditions were retained. Under combined optimized conditions, cumulative hydrogen production reached 194.86 mmol L^{-1}. Supplementation with AgNPs resulted in a slight, non-significant enhancement, with the highest yield (198.28 mmol L^{-1}) observed at 0.08 g L^{-1}, while higher concentrations exhibited inhibitory effects. Overall, the findings highlight the importance of strain selection and process optimization in enhancing photofermentative biohydrogen production and demonstrate the limited but concentration-dependent influence of nanoparticles.

Keywords : *Biohydrogen production; Purple non-sulfur bacteria; Rhodopseudomonas palustris; Photofermentation; Silver nanoparticles*

© 2026 Penerbit UTM Press. All rights reserved

1.0 INTRODUCTION

The global economy and modern society remain heavily reliant on fossil fuels, leading to escalating challenges, including rising energy costs, resource depletion, and severe environmental degradation. Growing global energy demand, combined with the finite nature of fossil reserves, has intensified concerns regarding long-term energy security (Mona et al., 2024; Russo et al.,

2026). The combustion of fossil fuels contributes substantially to atmospheric carbon dioxide (CO_2) emissions, which drive global warming and environmental pollution (Abd-Alla et al., 2025). In response, the transition to sustainable, low-carbon energy alternatives has become an international priority. Among the various renewable energy options, bioenergy derived from biological resources offers a promising pathway to reduce dependence on fossil fuels while promoting circular and sustainable energy systems (Kharisma et al., 2022).

Hydrogen (H_2) has emerged as a particularly attractive energy carrier due to its high energy density and its clean combustion by-product (water) making it central to the global vision for carbon-neutral energy (Elazab et al., 2025). However, industrial-scale hydrogen production still relies predominantly on fossil-based routes such as steam methane reforming and coal gasification, which are energy-intensive and environmentally harmful (Akpasi et al., 2025; Elazab et al., 2025). This has driven growing interest in biological hydrogen production, a process that uses microorganisms to convert organic substrates into hydrogen under environmentally benign conditions.

Among biological hydrogen producers, purple non-sulfur bacteria (PNSB) are among the most versatile and efficient groups for photofermentative hydrogen generation. PNSB are members of the α- and β-Proteobacteria distinguished by the presence of bacteriochlorophylls and carotenoids that give them their characteristic purple to reddish pigmentation. They perform anoxygenic photosynthesis under anaerobic conditions using near-infrared light, converting a wide range of organic substrates, including organic acids, alcohols, and fatty acids, into hydrogen and other metabolites (Bayon-Vicente et al., 2025; Sakarika et al., 2020).

A hallmark of PNSB metabolism is its flexibility: cells can grow photoautotrophically, photoheterotrophically, or chemoheterotrophically depending on environmental cues. This adaptability allows them to thrive in diverse and often polluted habitats, making them ideal candidates for bioenergy applications that utilize organic waste streams (Asif et al., 2021; Morrison & Bose, 2024; Sakarika et al., 2020). Several well-studied PNSB species, including *Rhodopseudomonas palustris*, *Rhodobacter sphaeroides*, *Rhodospirillum rubrum*, and *Rhodobacter capsulatus*, are known to produce hydrogen via the nitrogenase-mediated reduction of protons during photofermentation (Hu et al., 2018; Sagir et al., 2017; Zhang et al., 2023). This process not only contributes to renewable hydrogen generation but also represents a sustainable biological route for waste valorization (Gupta et al., 2024).

Despite its potential, biohydrogen production using PNSB is often constrained by low yields, slow production rates, and the sensitivity of nitrogenase activity to environmental conditions, including pH, temperature, substrate type, and nutrient availability (Maturi et al., 2026; Yildirim & Ozkaya, 2025). These limitations underline the need for strain-level optimization of cultivation parameters to maximize hydrogen output. Moreover, advances in nanobiotechnology have introduced new strategies to enhance microbial metabolism using metallic nanoparticles. Nanoparticles such as silver (AgNPs), gold, and nickel can act as biocatalysts or electron mediators, facilitating proton–electron transfer and stimulating enzyme activity (Abdul Aziz et al., 2022; Yildirim & Ozkaya, 2025). In particular, silver nanoparticles (AgNPs) have drawn attention for their high electron conductivity and surface reactivity, which may stabilize metabolic activity even in stress-prone fermentation systems (Dogmaz & Cavas, 2023; Iwuji et al., 2024).

The present study investigates the biohydrogen production capacity of PNSB strains isolated from the polluted Sungai Kim Kim River (Johor, Malaysia), a site known for its high organic and heavy-metal loads. Two morphologically distinct isolates were preliminarily screened; one strain (PNSB_P) produced measurable hydrogen, while the other (PNSB_B) did not under identical conditions. The biohydrogen-producing strain was therefore selected for detailed physiological characterization and process optimization. Key growth parameters such as inoculum size, carbon source, temperature, and growth condition were systematically optimized using the one-factor-at-a-time (OFAT) approach to identify conditions that maximize hydrogen yield.

Finally, the effects of silver nanoparticle supplementation on hydrogen production under optimized conditions were evaluated.

This integrated approach, spanning strain identification, laboratory-scale optimization, and nanoparticle-based enhancement, aims to characterize locally isolated PNSB from a contaminated tropical environment, determine their biohydrogen production potential under photofermentative conditions, identify key operational parameters that influence yield, and assess the effects of AgNPs on hydrogen production kinetics. The findings contribute to the development of locally isolated PNSB for sustainable bioprocesses for renewable hydrogen generation and highlight the potential of nanomaterials to enhance microbial energy conversion efficiency.

2.0 MATERIALS AND METHODS

2.1 Isolation and cultivation

Two previously isolated and uncharacterized purple non-sulfur bacteria (PNSB) strains were obtained from the polluted Sungai Kim Kim River, Pasir Gudang, Malaysia, and preserved in glycerol stocks prior to use. For revival, two different growth media, purple non-sulfur bacteria enrichment medium (PNSBEM) and basal medium (BM), were prepared and used under identical cultivation conditions. The PNSBEM consisted of ammonium chloride (1.0 g), disodium hydrogen phosphate (0.5 g), sodium

chloride (2.0 g), magnesium chloride (0.2 g), 80% sodium lactate (6 mL), and yeast extract (2.0 g) dissolved in 1000 mL of distilled water. The BM was composed of potassium dihydrogen phosphate (0.33 g), magnesium sulfate (0.33 g), sodium chloride (0.33 g), ammonium chloride (0.50 g), calcium chloride (0.05 g), sodium succinate (1.00 g), yeast extract (0.02 g), and 0.02% iron (II) sulfate (0.50 g) prepared in 1000 mL of distilled water.

For each culture, 18 mL of sterile medium and 2 mL (10% v/v) inoculum were mixed in 36 mL serum bottles (total working volume = 20 mL). The bottles were sealed with butyl rubber stoppers and crimped with aluminium caps, then sparged with nitrogen gas for 3 min to establish anaerobic conditions. Incubation was performed at 30 °C under continuous illumination (2–3 klux) until a characteristic purple bloom appeared. Strains grown in PNSBEM and BM were designated as PNSB_P and PNSB_B, respectively.

2.2 Morphological and Molecular Characterization

Colony morphology was assessed by streaking the cultures onto agar plates containing their respective media, followed by incubation at 30°C under continuous light for 18 hours. Colony characteristics were then visually examined. For microscopic analysis, a single colony was suspended in sterile water, heat-fixed onto a glass slide, and subjected to Gram staining. The stained samples were observed under a light microscope to determine cellular morphology and Gram reaction.

Thereafter, genomic DNA was extracted from PNSB samples using the Promega Wizard™ Genomic DNA Extraction Kit, following the protocol described by Liu et al. (2021). The extracted DNA was quantified using a NanoDrop 100 spectrophotometer, with DNA concentration and purity assessed based on absorbance ratios at 260/280 nm and 260/230 nm.

The 16S rRNA gene was amplified by polymerase chain reaction (PCR) in a total reaction volume of 25 µL. The reaction mixture comprised 1.0 µL each of forward primer (5'-AGA GTT TGA TCC TGG CTC AG-3) and reverse primer (5'-AAG GAG GTG ATC CAG CC-3) (Webster et al., 2009) at a final concentration of 0.4 µM, 1.5 µL of DNA template (<250 ng), 12.5 µL of master mix (1×), and 9.0 µL of nuclease-free water. PCR amplification was performed using an Eppendorf PCR Master Cycler with an initial denaturation at 94°C for 5 minutes, followed by denaturation at 94°C for 1 minute, annealing at 55°C for 1 minute, and extension at 72°C for 4 minutes, with a final extension step at 72°C for 10 minutes.

PCR products were analyzed by 1% agarose gel electrophoresis using Midori Green Advanced DNA stain. Samples and a DNA ladder were loaded into the gel and electrophoresed, and the bands were visualized using a BIORAD ChemiDoc™ Touch Imager to confirm the expected fragment size. Verified PCR products were subsequently sent to Apical Scientific Sdn. Bhd. for 16S rRNA gene sequencing.

The obtained forward and reverse sequences were assembled into full-length sequences using BioEdit software. Sequence identification was performed using the Basic Local Alignment Search Tool (BLAST) to determine similarity with reference sequences. Multiple sequence alignment and phylogenetic analysis were conducted using Molecular Evolutionary Genetics Analysis version 11 (MEGA 11), where a neighbor-joining phylogenetic tree was constructed with bootstrap analysis to assess the reliability of the tree topology (Posada & Crandall, 2021).

2.3 Bacterial Growth Profile and Kinetic Analysis

The growth profile of the PNSB was evaluated through dry cell weight (DCW) determination, optical density (OD) measurement, and kinetic analysis. For DCW determination, the procedure was carried out according to Johari (2022). 2 mL microcentrifuge tubes were pre-dried in an incubator at 90°C overnight, cooled at room temperature for 30 minutes, and weighed. Bacterial cultures (1.5 mL) collected at different incubation times (24, 48, 55, 60, 65, 72, 96, and 120 hours) were transferred into the pre-weighed tubes and centrifuged at 20,000 rcf for 10 minutes. The supernatant was carefully removed, and the step was repeated using an additional 1.5 mL of culture to ensure sufficient biomass was collected. The resulting pellet was washed with 1.5 mL of deionized water, then centrifuged at 20,000 rcf for 10 minutes, and the supernatant was removed. The tubes were then dried at 40°C overnight, cooled for 30 minutes, and reweighed. The dry cell weight was calculated by subtracting the initial tube weight from the final weight of the tube containing the dried biomass.

Optical density measurements were performed to monitor cell growth over time. For each sampling interval, cultures were analyzed at 600 nm using a UV–Vis spectrophotometer.

A calibration curve relating DCW and OD_{600} was used to estimate biomass during subsequent experiments. Specific growth rate (µ), maximum specific growth rate (μ_{max}), and doubling time (td) were calculated from exponential phase data.

2.4 Biohydrogen Quantification

Biohydrogen production by the PNSB isolates was screened using gas chromatography equipped with a thermal conductivity detector (GC-TCD). Gas samples (1 mL) were withdrawn from the headspace of serum bottles using an airtight glass syringe

(Agilent) and injected into the GC-TCD system. The oven temperature was maintained at 60°C, while both the front and back detectors were set to 250°C. Argon and helium were used as carrier gases at a flow rate of 18 mL/min.
Hydrogen concentration (mol L^{-1}) was calculated from the chromatogram peak area using the standard-curve relationship:

$$H_2\,(\text{mol L}^{-1}) = \frac{A_{(\text{standard})}}{A_{(\text{sample})}} \times mole\ fraction$$

Where A_{standard} represents the surface area of the gas peak in the standard chromatogram (2576), and A_{sample} represents the surface area of the gas peak in the sample chromatogram. The mole fraction of H_2 in the standard was 0.0164 mol/L.

2.5 Screening of Isolates for Biohydrogen Production

Both isolates (PNSB_P and PNSB_B) were cultivated under identical conditions, and hydrogen accumulation was monitored for up to 120 h. Only PNSB_P (identified as *Rhodopseudomonas palustris*) produced measurable hydrogen; therefore, this strain was used for subsequent optimization and nanoparticle supplementation experiments.

2.6 Baseline Biohydrogen Production

Baseline hydrogen production by *R. palustris* PNSB_P was evaluated over a 7-day (168 h) cultivation period to establish the unoptimized hydrogen yield profile. Gas samples were collected at predetermined time intervals and analyzed via GC–TCD to quantify hydrogen concentration.

2.7 OFAT-Based Optimization of Culture Conditions

The one-factor-at-a-time (OFAT) approach was employed to optimize parameters influencing biohydrogen production by *Rhodopseudomonas palustris* PNSB_P. Unless otherwise stated, all experiments were conducted under standard anaerobic illuminated conditions.

The effect of inoculum size was evaluated at 5%, 10%, and 15% (v/v). Growth conditions were subsequently assessed by comparing anaerobic light (with N_2 sparging) and facultative anaerobic light (without sparging). Biohydrogen production was measured over an incubation period of 48–72 hours.

For carbon source optimization, sodium lactate in the standard PNSB enrichment medium was replaced with sodium succinate, fructose, or maltose, and hydrogen production was evaluated over the same incubation period. The influence of temperature was examined at 30 °C, 37 °C, and 40 °C under identical conditions and time intervals.

This optimization strategy enabled the identification of key factors affecting biohydrogen production and the determination of conditions that maximize hydrogen yield by the isolated PNSB strain.

2.8 Effect of Silver Nanoparticles on Biohydrogen Production

The optimized conditions determined by OFAT were applied to assess the influence of silver nanoparticles (AgNPs) on hydrogen yield. Commercial AgNPs were dispersed in double-distilled water at 0.04, 0.08, and 0.12 g L^{-1}, ultrasonicated for 30 min for uniform suspension, and aseptically added to the enrichment medium prior to inoculation. A control (0 g L^{-1} AgNPs) was also run. Cultivation and hydrogen analysis followed the same procedures as previously described. Growth was concurrently monitored by OD_{660} measurements to evaluate any inhibitory or stimulatory effects.

2.9 Data analysis

All experiments were conducted in triplicate, and results are reported as mean ± standard deviation. Statistical analyses and graphs were prepared using Microsoft Excel 365. One-way analysis of variance (ANOVA) was performed to test for significant differences among treatments, with $p < 0.05$ considered statistically significant.

3.0 RESULTS AND DISCUSSION

3.1 Characterization of isolates

The retrieved unknown strains, PNSB_P and PNSB_B, were successfully revived under anaerobic light conditions until a characteristic bloom was observed, indicating active growth. PNSB_P exhibited a gradual change from a pale pink broth to an intense red coloration. In contrast, PNSB_B showed a slower response, with the medium changing from colourless to light pink, as shown in Figure 1.A and 1.D. This observable colour development is attributed to the synthesis of photosynthetic pigments, primarily bacteriochlorophylls and carotenoids, which are hallmarks of purple non-sulfur bacteria and play a critical role in light harvesting during anoxygenic photosynthesis (Dhar et al., 2023).

The morphological characteristics differed between the two strains, with PNSB_P displaying irregular rod-shaped cellsande PNSB_B exhibiting an ovoid morphology (Figure 1.B and 1.E). Such morphological diversity is commonly reported among PNSB species and reflects their broad physiological and taxonomic diversity (Sakarika et al., 2019). Microscopic examination at 1000× magnification (Figures 1.C and 1.F) revealed that both isolates were Gram-negative, indicated by their pink staining. This is consistent with the typical cell wall structure of Gram-negative bacteria, which possess a thin peptidoglycan layer and an outer lipid membrane that does not retain crystal violet during Gram staining (Tripathi et al., 2025). These preliminary observations provide an initial indication of strain-specific characteristics.

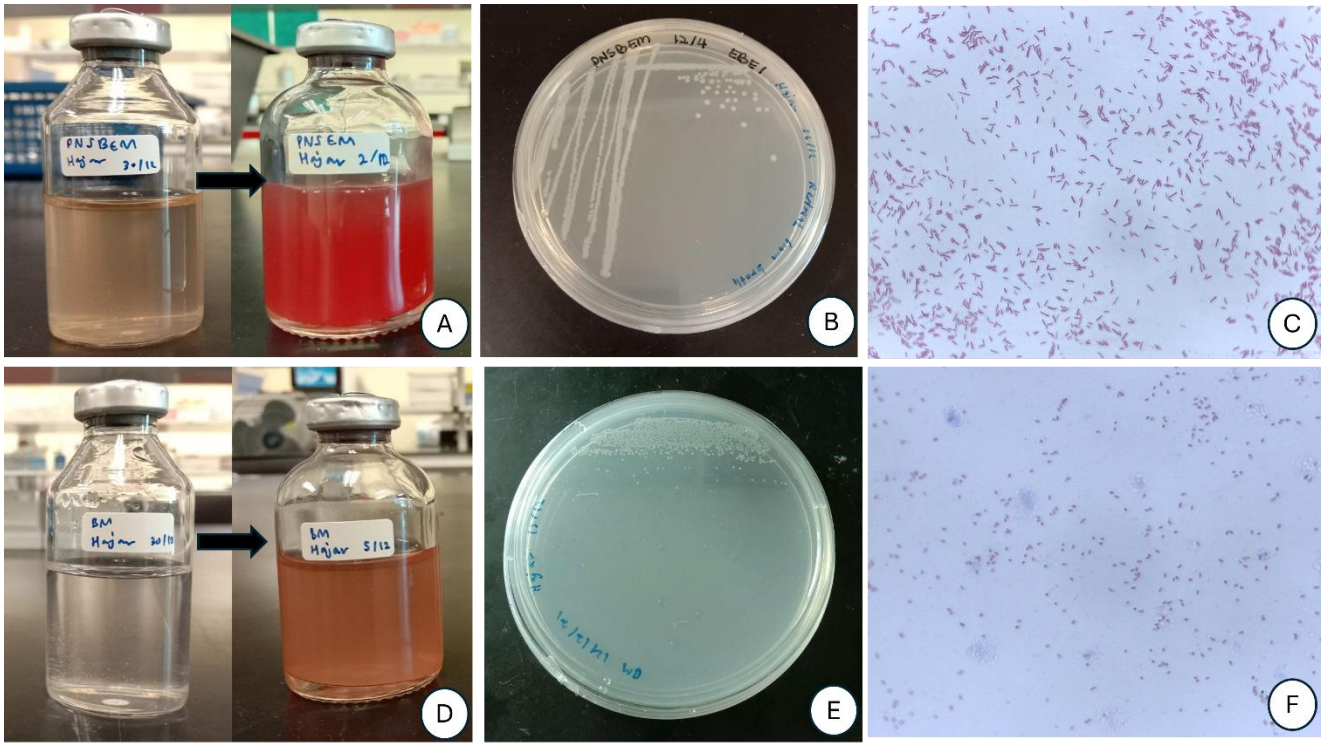


Figure 1 : Comparison of Purple Non-Sulfur Bacteria (PNSB) isolates in liquid culture, solid agar, and under microscopic observation. After 7 days of incubation at 30 °C under continuous illumination (2–3 klux), the horizontal top row (A, B, C) represents strain PNSB_P, while the bottom row (D, E, F) represents strain PNSB_B

The successful isolation, revival, and pigmentation of the two bacterial strains confirm their identity as purple non-sulfur bacteria (PNSB), as pigment synthesis is a defining functional trait linked to photosynthetic activity and light-harvesting capability. The more rapid and intense pigmentation observed in PNSB_P suggests enhanced development of the photosynthetic apparatus, likely reflecting higher bacteriochlorophyll and carotenoid activity, which are essential for light absorption and energy conversion in photofermentative systems. Such variations in pigmentation have been associated with improved metabolic performance and biohydrogen production potential in PNSB (Rashid et al., 2022).

3.2 DNA quality assessment and Gel electrophoresis

Genomic DNA extracted from PNSB_P and PNSB_B was assessed for concentration and purity using a NanoDrop spectrophotometer. As summarized in Table 1, PNSB_B exhibited a higher DNA concentration (509.4 ng/μL) compared to PNSB_P (174.2 ng/μL), indicating variation in biomass yield or extraction efficiency between the two isolates. DNA purity was evaluated based on A260/A280 and A260/A230 absorbance ratios, which are commonly used indicators of protein and organic

contaminant presence, respectively. According to established standards, pure DNA typically exhibits an A260/A280 ratio of approximately 1.8 and an A260/A230 ratio of 2.0–2.2 (Armbrecht, 2013).

Both PNSB_P and PNSB_B exhibited absorbance ratios within or near the acceptable range, indicating minimal contamination and suitable DNA quality for downstream molecular analysis. The slightly elevated A260/A280 value observed for PNSB_P (2.14) may suggest minor RNA contamination, although it remains acceptable for PCR-based applications (Lucena-Aguilar et al., 2016). Overall, the DNA samples were considered sufficiently pure for successful amplification of the target gene.

The integrity and successful amplification of the 16S rRNA gene were subsequently verified via agarose gel electrophoresis. Distinct bands corresponding to approximately 1500 base pairs were observed for both PNSB_P and PNSB_B, confirming successful PCR amplification of the target gene region. The observed fragment size is consistent with the expected length of the bacterial 16S rRNA gene, which is widely used for taxonomic identification and phylogenetic analysis (de Souza et al., 2025).

The presence of clear and well-defined bands without significant smearing further indicates good DNA integrity and efficient amplification. This confirms that the extracted DNA was of adequate quality for sequencing and subsequent phylogenetic analysis. These results provide a reliable foundation for accurate identification of the isolates and support further investigation into their biohydrogen production potential (Bartoš et al., 2024).

Table 1 : Concentration and purity of DNA from sample PNSB_P and PNSB_B

Sample	DNA concentration (ng/µL)	A260/A280	A260/A230
PNSB_P	174.2	2.14	2.06
PNSB_B	509.4	1.89	1.89

3.3 Molecular identification and phylogenetic analysis

The full-length 16S rRNA gene sequences obtained for PNSB_P and PNSB_B were analyzed using the Basic Local Alignment Search Tool (BLAST) to determine their taxonomic identity based on sequence similarity with database entries. The BLAST results revealed that PNSB_P shared 99.51% sequence similarity with *Rhodopseudomonas palustris*, indicating a high level of confidence in species-level identification. In contrast, PNSB_B exhibited a lower similarity of 81.27% to *Rhodopseudomonas* sp. NTUIOB TPP6, suggesting that it may represent a more distantly related or potentially novel strain within the genus (Hackmann, 2025).

To further validate these findings, sequence alignment and phylogenetic analysis wereperformted using MEGA 11. As illustrated in Figure 2, both isolates clustered within the class *Alphaproteobacteria*, specifically within the genus *Rhodopseudomonas.* PNSB_P showed strong clustering with *Rhodopseudomonas palustris*, supported by a 100% bootstrap value, which is consistent with the BLAST identification. In contrast, PNSB_B exhibited weaker phylogenetic resolution, with a bootstrap support of 54% and clustering near *Rhodopseudomonas oryzae* and *Rhodopseudomonas thermotolerans*. This lower confidence suggests greater genetic divergence and reinforces the possibility that PNSB_B may represent a less characterized or novel strain within the genus.

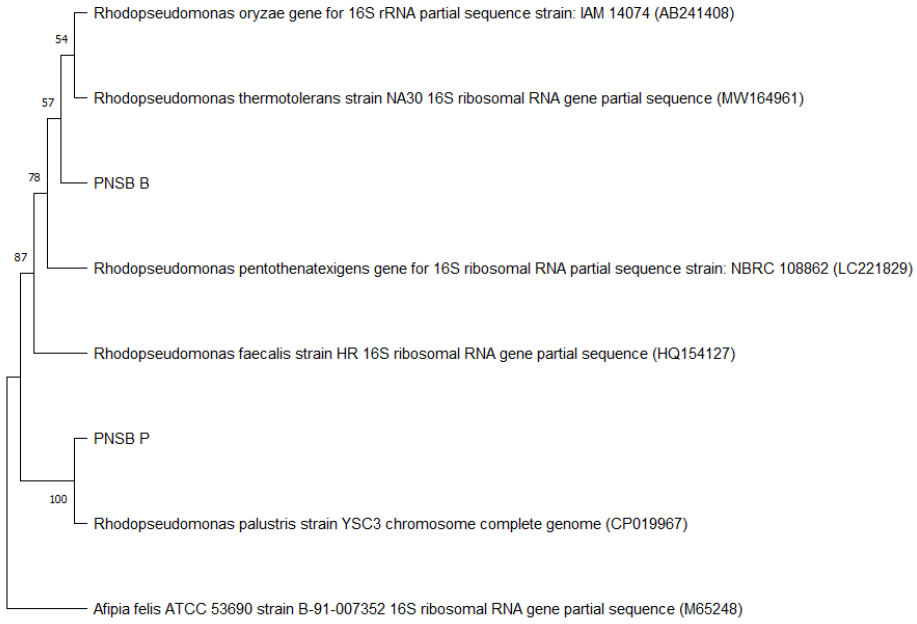


Figure 2 : Neighbour-joining phylogenetic tree for PNSB_P and PNSB_B with related strains of PNSB based on 16s rDNA gene sequences. The tree was constructed using the neighbor-joining algorithm with 100 bootstraps. Afipia felis (M65248) was selected as the outgroup to root the tree.

Molecular identification further revealed that PNSB_P is closely related to *Rhodopseudomonas palustris*, a species widely recognized for its metabolic versatility and efficiency in photofermentative hydrogen production. In contrast, the lower phylogenetic resolution observed for PNSB_B suggests that it may represent a more genetically distinct or less-characterized strain. This distinction is important, because previous studies have demonstrated that even closely related PNSB strains can exhibit substantial variation in hydrogen-producing capabilities due to differences in genomic architecture, redox-balancing mechanisms, and regulation of nitrogenase activity (McKinlay, 2014; Navid et al., 2019). Recent systems-level analyses further indicate that PNSB strains respond differently to environmental stresses by redirecting metabolic fluxes toward alternative pathways, thereby influencing hydrogen yields (Huang & Zhou, 2026).

3.4 Screening of Isolates for Biohydrogen Production

Preliminary screening of biohydrogen production was conducted to evaluate the hydrogen-producing capabilities of the isolated strains. PNSB_P exhibited measurable hydrogen evolution, whereas no detectable hydrogen production was observed in PNSB_B, indicating a clear variation in hydrogen-producing potential between the two isolates.

Based on these findings, PNSB_P was selected for subsequent optimization and nanoparticle supplementation studies due to its demonstrated ability to produce biohydrogen. Notably, *Rhodopseudomonas palustris*, to which PNSB_P is closely related, is one of the most extensively studied and well-established model organisms for photofermentative hydrogen production (Bosman et al., 2023). Table 2 summarizes the characteristics of both isolates.

Table 2 : Summary of characteristics of PNSB_P and PNSB_B isolates.

Characteristic	**PNSB_P**	**PNSB_B**
Gram reaction	Negative	Negative
Cell morphology	Rod	Coccoid
16S rRNA identification	*Rhodopseudomonas palustris* (99.51%)	*Rhodopseudomonas* sp. (81.27%)
Biohydrogen production	Detected	Not detected

This confirmed that only PNSB_P exhibited biohydrogen-producing capability, while PNSB_B showed no detectable hydrogen production despite active growth. This finding highlights the strong strain dependency of hydrogen production in PNSB, which is primarily governed by the presence, regulation, and metabolic integration of nitrogenase pathways. Similar observations have been widely reported, where closely related phototrophic bacteria display markedly different hydrogen-

producing capacities under identical conditions. For instance, comparative studies have shown that *Rhodopseudomonas palustris* and *Rhodopseudomonas* spp. were capable of hydrogen production from volatile fatty acids, whereas *Rubrivivax* spp. assimilated the same substrates without any detectable H_2 evolution, indicating a preferential allocation of reducing equivalents toward biomass formation rather than nitrogenase activity (Wu et al., 2010). Similarly, *Rhodospirillum rubrum* has been reported to exhibit negligible biomass accumulation and no hydrogen production under conditions optimized for photofermentation, while certain *R. palustris* strains (e.g., AV33) produce only minimal hydrogen due to diversion of carbon flux toward storage compounds such as poly-β-hydroxybutyrate (PHB) (Bianchi et al., 2010). These findings collectively demonstrate that hydrogen production is not a universal trait among PNSB but is highly dependent on strain-specific metabolic regulation, particularly the balance between energy storage, biomass synthesis, and nitrogenase-mediated electron disposal pathways.

3.5 Comparative Growth Kinetics of *Rhodopseudomonas* Isolates

A strong linear correlation between optical density (OD_{600}) and dry cell weight (DCW) was established for both isolates. The coefficients of determination (R^2) were 0.9908 for PNSB_P and 0.9700 for PNSB_B, with corresponding regression equations of $y = 0.333x$ and $y = 0.4351x$, respectively. These results indicate that optical density is a robust proxy for biomass estimation, consistent with previous findings (Choe et al., 2025a).

Kinetic analysis revealed that PNSB_B exhibited higher specific growth rate ($\mu = 0.2414\ h^{-1}$) and maximum specific growth rate ($\mu_{max} = 0.4828\ h^{-1}$) compared to PNSB_P ($\mu = 0.1244\ h^{-1}$; $\mu_{max} = 0.2488\ h^{-1}$), indicating faster cell proliferation and substrate utilization. However, despite its slower growth, PNSB_P achieved a higher maximum biomass yield (0.0063 g L^{-1} h^{-1}) and a slightly shorter doubling time (2.79 h) than PNSB_B (0.0017 g L^{-1} h^{-1}; 2.87 h). The correlation coefficients and kinetic parameters are summarized in Table 1.

Table 3 : Growth kinetic parameters of *Rhodopseudomonas* isolates

Isolate	μ (hr^{-1})	μ_{max} (hr^{-1})	T_d (h)	X_{max} (g/l/h)	R^2
Rhodopseudomonas palustris PNSB_P	0.1244	0.2488	2.7857	0.0063	0.9908
Rhodopseudomonas sp. PNSB_B	0.2414	0.4828	2.8711	0.0017	0.9700

Note: μ = specific growth rate; μ_{max} = maximum specific growth rate; T_d = doubling time; X_{max} = maximum biomass.

The growth profiles of both isolates followed typical bacterial dynamics, although no distinct lag phase was observed, likely due to the use of actively growing inoculum and consistent culture conditions (Martínez et al., 2023). PNSB_P exhibited exponential growth between 24 and 65 h, followed by a transition into the stationary phase, while PNSB_B showed a prolonged exponential phase extending up to 96 h. Although PNSB_B displayed higher specific growth rates, this did not translate into improved hydrogen production. Instead, PNSB_P achieved higher biomass productivity and biohydrogen output, highlighting the commonly reported trade-off between growth rate and metabolite production. Rapidly growing cells tend to allocate energy toward biomass formation, whereas slower-growing systems often redirect reducing equivalents toward secondary metabolic processes such as hydrogen evolution (Ramin & Allison, 2019).

The strong linear relationship observed between optical density (OD_{600}) and dry cell weight (DCW) ($R^2 > 0.97$) confirms OD as a reliable proxy for biomass estimation, consistent with previous reports for *Rhodopseudomonas* and *Rhodobacter* species under stable physiological conditions (Choe et al., 2025b; Wang et al., 2022). This linearity reflects consistent pigment synthesis and light-harvesting characteristics during exponential growth, indicating metabolic stability and efficient energy utilization. The kinetic parameters obtained for PNSB_P ($\mu = 0.1244\ h^{-1}$; $\mu_{max} = 0.2488\ h^{-1}$) fall within the typical range reported for *R. palustris* (0.10–0.30 h^{-1}) under photoheterotrophic conditions, supporting its suitability for biohydrogen production (Bosman et al., 2023).

3.6 Baseline Biohydrogen Production

Baseline biohydrogen production by *R.palustris* PNSB_P was evaluated over a 7-day (168 h) cultivation period to establish the unoptimized hydrogen yield profile (Figure 3). Hydrogen production increased rapidly during the initial incubation phase, rising from 1.5 mmol/L at 24 h to a maximum of 5.08 mmol/L at 48 h, followed by a decline to 2.9 mmol/L at 72 h and fluctuating thereafter, reaching 3.2 mmol/L at 96 h and 4.51 mmol/L at 120 h before dropping to lower levels at 144 h (1.4 mmol/L) and 168 h (1.7 mmol/L).

Based on this baseline profile, the t 48–72 h time range was identified as the most critical period for hydrogen production, corresponding to the transition between the exponential and stationary growth phases. This interval was therefore selected to guide incubation time points in subsequent one-factor-at-a-time (OFAT) optimization experiments aimed at maximizing hydrogen yield.

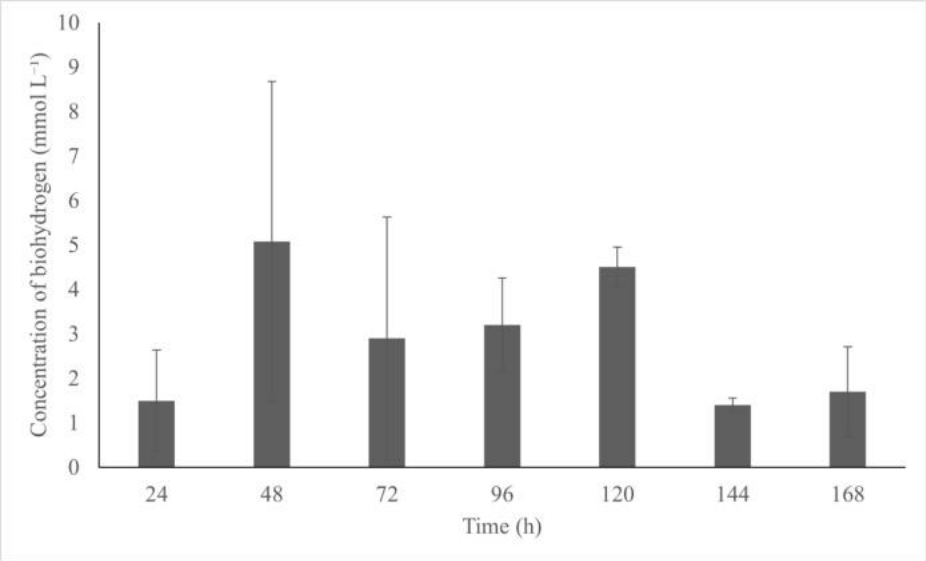


Figure 3 : Time-course profile of biohydrogen production by *Rhodopseudomonas palustris*.

The observed biohydrogen production pattern, characterized by a rapid increase followed by a gradual decline, is consistent with typical batch photofermentation behaviour in PNSB systems. Hydrogen production is closely linked to active cellular metabolism and typically peaks during the late exponential phase, then declines due to substrate depletion, accumulation of inhibitory by-products, or a shortage of reducing equivalents (Jiang et al, 2023). The peak observed at 48 h aligns with previous studies on *R. palustris* and *Rhodobacter sphaeroides*, wherein the maximum hydrogen evolution typically occurs between 36 and 60 h under batch conditions (Bosman et al., 2023; Tiang et al., 2024)

3.6 Effect of Cultivation Parameters on Biohydrogen Production

We evaluated the biohydrogen production performance of Rhodopseudomonas palustris PNSB_P under varying cultivation parameters using a one-factor-at-a-time (OFAT) approach. The factors examined, inoculum size, growth condition, carbon source, and incubation temperature, are known determinants of hydrogen production efficiency in photofermentative systems (Monir et al., 2022).

The optimization results (Figure 4) revealed that inoculum size of 5% (v/v) yielded the highest cumulative biohydrogen production (14.52 ± 3.31 mmol L^{-1}), compared to 15% (13.82 ± 4.10 mmol L^{-1}) and 10% (13.49 ± 2.46 mmol L^{-1}). Among the carbon sources tested, maltose resulted in the highest hydrogen yield (83.21 ± 1.34 mmol L^{-1}), markedly exceeding fructose (46.09 ± 1.79 mmol L^{-1}), lactate (23.37 ± 5.16 mmol L^{-1}), and succinate (12.51 ± 2.71 mmol L^{-1}). Under different growth conditions, light anaerobic culture produced 21.57 ± 3.66 mmol L^{-1} H_2, which was approximately 5-fold higher than that obtained under light facultative conditions (4.26 ± 0.50 mmol L^{-1}). Temperature optimization showed a progressive increase in hydrogen production with rising temperature, from 109.54 ± 2.18 mmol L^{-1} at 30 °C to 132.14 ± 4.83 mmol L^{-1} at 37 °C, reaching a maximum of 136.06 ± 5.20 mmol L^{-1} at 40 °C.

Only the carbon source and growth conditions significantly affected biohydrogen yield ($p < 0.05$). Although a 5% inoculum and 40 °C yielded higher hydrogen production, the differences were not statistically significant ($p = 0.959$, $p = 0.294$).

Therefore, subsequent experiments used maltose under light–facultative conditions, maintaining baseline inoculum (10%) and temperature (30 °C).

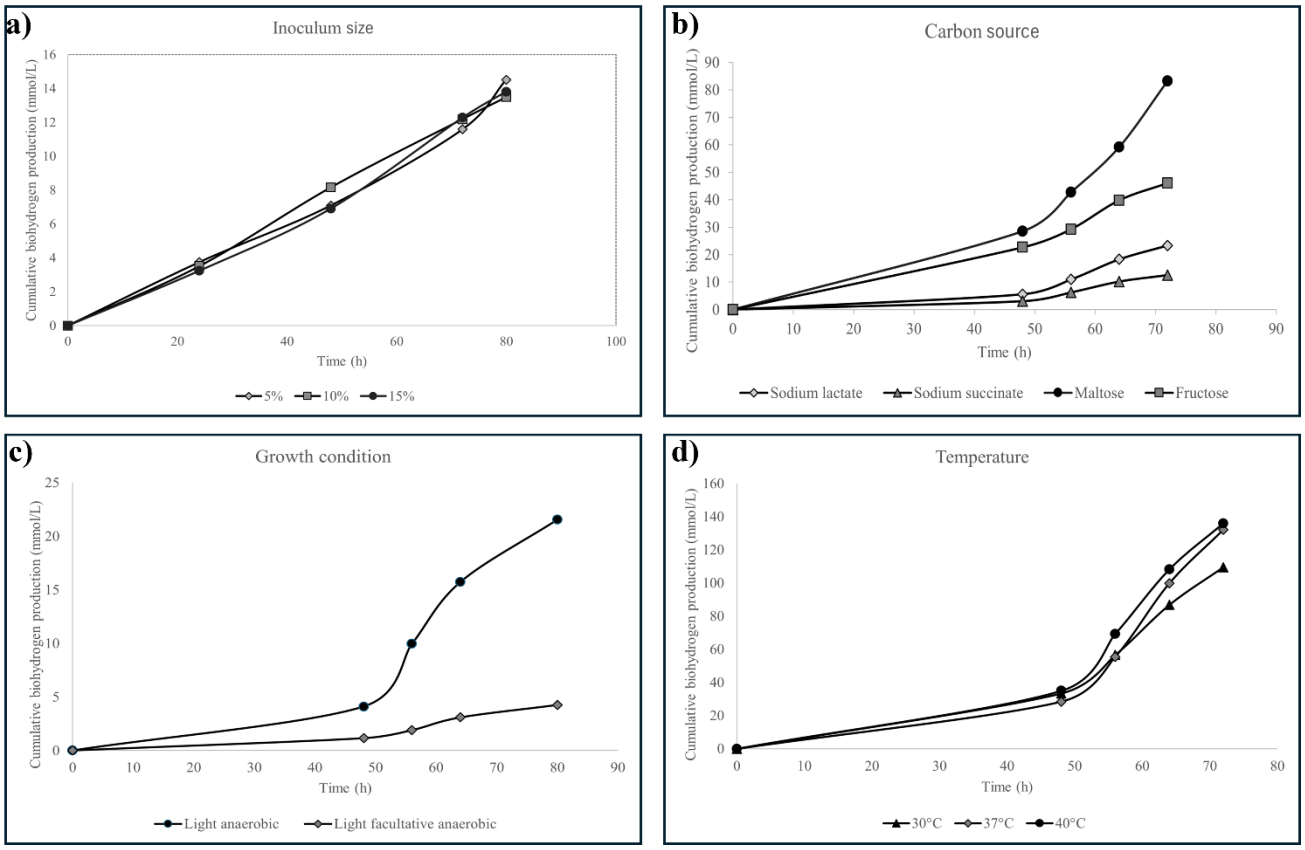


Figure 4 : Effects of cultivation parameters on cumulative biohydrogen production by *Rhodopseudomonas palustris* PNSB_P under photofermentative conditions: (a) inoculum size (b) carbon source (c) growth condition, and (d) incubation temperature

Optimization using the one-factor-at-a-time (OFAT) approach revealed that the carbon source and growth conditions significantly influenced hydrogen production, whereas inoculum size and temperature showed no statistically significant effects. Within the tested range (5–15%), inoculum size had minimal impact on hydrogen yield, consistent with previous findings that inoculum density primarily affects the duration of the lag phase rather than overall productivity when maintained within optimal limits (Laurinavichene & Tsygankov, 2018). Studies on PNSB photofermentation have shown that moderate inoculum sizes (typically 5–15%) can accelerate the onset of hydrogen production by increasing the initial biomass concentration but do not significantly enhance final hydrogen yield because of limitations imposed by light availability and substrate utilization (Ulhiza et al., 2022). Higher inoculum densities may even reduce specific hydrogen production rates due to increased competition for resources and self-shading. For example, statistical optimization studies have identified 5% inoculum as optimal, whereas higher levels, such as 15%, yielded no proportional gain in yield despite faster initiation of production. Conversely, studies in other systems, including *Parageobacillus* spp., reported optimal performance at intermediate inoculum levels (10%), while excessive inoculum (e.g., 20%) reduced hydrogen production rates by up to 48% due to metabolic overload (Mohr et al., 2019).

Growth conditions had a pronounced effect, with strict light–anaerobic conditions yielding significantly more hydrogen than light–facultative conditions. This result is consistent with the well-established oxygen sensitivity of nitrogenase, the key enzyme responsible for hydrogen evolution. Even low oxygen concentrations can irreversibly inhibit nitrogenase activity, thereby suppressing hydrogen production (Stal, 2017).

Carbon source was identified as the most influential parameter, with maltose yielding significantly higher hydrogen production than fructose, lactate, and succinate. This finding supports the evidence that *R. palustris* exhibits greater substrate versatility and can efficiently utilize carbohydrates to enhance reducing power generation (Hu et al., 2018). The superior performance of maltose likely reflects enhanced NADH availability and ATP generation, which are critical for nitrogenase-driven hydrogen production (Cha et al., 2025).

Temperature optimization showed an increasing trend in hydrogen production at elevated temperatures (37–40 °C), although the differences were not statistically significant. While 30 °C is widely reported as the optimal temperature for many PNSB species, several studies have demonstrated enhanced hydrogen production at higher temperatures in adapted strains of *R. palustris*, with the optimal temperature shifting to 35–40 °C. For instance, Lo et al. (2012) reported that the engineered strain CGA-CThydA achieved optimal hydrogen production at 40 °C, exhibiting a 2.07-fold increase in production rate compared to control conditions and a different study reported 4-fold higher hydrogen production by strain ATH2.1.37 at 40 °C compared to

the control, 30 °C (du Toit & Pott, 2021). This supports the observed trend in the present study, suggesting that elevated temperatures may enhance enzymatic activity and metabolic flux toward hydrogen production, particularly in strains with thermal adaptability or modified hydrogenase systems. Nevertheless, the lack of statistical significance in the current results indicates that the isolate maintains stable photofermentative performance across a mesophilic range, highlighting its metabolic robustness rather than strict temperature dependence.

When the optimized parameters were combined, a substantial increase in hydrogen production (194.86 mmol L^{-1}) was observed, demonstrating the synergistic interaction of multiple operational factors. This enhancement reflects the cumulative effects of improved substrate utilization, optimized redox balance, and favorable environmental conditions that collectively promote nitrogenase-driven hydrogen evolution. Such synergistic improvements are widely reported in the literature, where multi-parameter optimization consistently yields higher hydrogen yields than individual-actor optimization alone. (Al-Mohammedawi et al., 2018; Gokfiliz-Yildiz & Karapinar, 2018). These findings highlight the importance of integrated process optimization, as biohydrogen production in PNSB systems is governed by the interplay of metabolic and environmental variables rather than any single limiting factor. Notably, baseline conditions (10% inoculum and 30 °C) were retained for parameters that showed no significant differences, ensuring experimental consistency and avoiding overinterpretation of marginal improvements.

3.7 Effect of Silver Nanoparticles on Biohydrogen Production

When the parameters from the OFAT experiments were combined, cumulative biohydrogen production increased to 194.86 ± 6.15 mmol L^{-1}, corresponding to approximately 13.4-, 9.0-, 2.3-, and 1.4-fold increases relative to the individual optima for inoculum size, growth condition, carbon source, and temperature, respectively.

Subsequently, the effect of silver nanoparticles (AgNPs) was evaluated under these combined conditions (Figure 5). Hydrogen yields of 195.51 ± 5.62, 198.28 ± 3.68, and 185.56 ± 6.99 mmol L^{-1} were obtained at AgNP concentrations of 0.04, 0.08, and 0.12 g L^{-1}, respectively, compared to 194.86 mmol L^{-1} for the control. However, no statistically significant differences were observed among treatments (ANOVA, $p > 0.05$).

Growth of *Rhodopseudomonas palustris* PNSB_P, monitored as optical density (OD_{600}) over 60 h (Figure 7), exhibited similar trends across all treatments. Optical density peaked between 0.45 and 0.47 during the exponential phase (approximately 25 h) in the control, 0.04 g L^{-1}, and 0.08 g L^{-1} treatments, followed by stabilization in the stationary phase. In contrast, the 0.12 g L^{-1} treatment showed a lower peak OD (~0.42) and slower recovery thereafter. Statistical analysis confirmed no significant differences among treatments (ANOVA, $p > 0.05$), indicating that AgNP supplementation did not significantly affect bacterial growth or hydrogen production under the tested conditions. A summary of cumulative biohydrogen production from the OFAT and AgNP experiments is presented in Table 3.

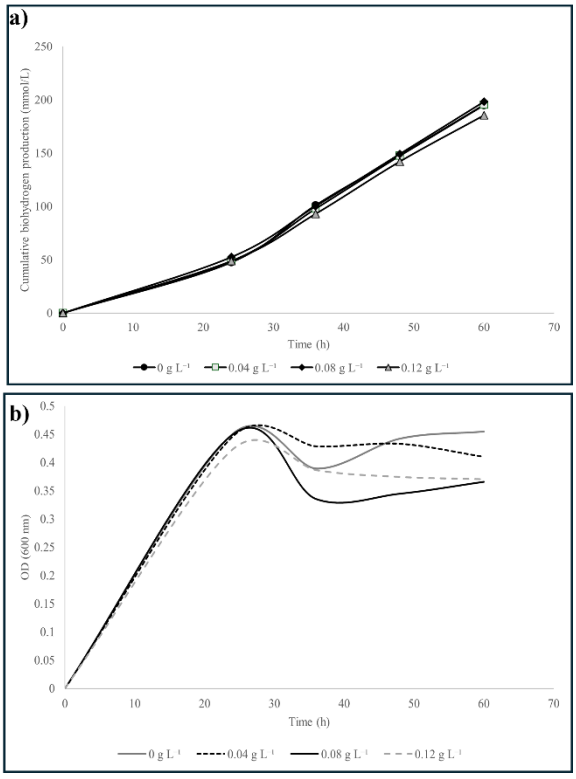


Figure 5 : Effect of silver nanoparticle concentration on a) biohydrogen production and b) bacterial growth

The addition of silver nanoparticles (AgNPs) resulted in a slight enhancement of hydrogen production at 0.08 g L^{-1}, although the effect was not statistically significant. This trend is consistent with the widely reported concentration-dependent behavior of nanoparticles in biohydrogen systems, where low concentrations stimulate microbial activity, whereas higher concentrations are inhibitory. At low concentrations, AgNPs can enhance electron transfer processes and improve redox balance by acting as conductive mediators, thereby facilitating hydrogenase or nitrogenase activity (Ashwini et al., 2024).

For example, Hellal et al. (2024) reported that core–shell nanosilver exhibited an optimal concentration of 40 mg/L, which significantly enhanced hydrogen yield (163 mL/g volatile solids) compared to the control (79 mL/g VS). However, further increasing the concentration to 50 mg/L resulted in strong inhibition of most bacterial populations in the sludge, demonstrating that exceeding the optimal threshold leads to pronounced cytotoxic effects. This inhibitory threshold is consistent with the present study, where AgNP supplementation at 0.12 g L^{-1} similarly led to a decline in hydrogen production relative to the lower concentration (0.08 g L^{-1}), indicating that higher nanoparticle loading may surpass the tolerance limit of the microbial system (Singla et al., 2022).

Similarly, green-synthesized silver oxide nanoparticles have been reported to enhance hydrogen production by approximately 17% at low concentrations (e.g., 400 µg L^{-1}), further supporting the stimulatory effect of sub-inhibitory nanoparticle doses on microbial hydrogen metabolism (Yildirim et al., 2022). However, beyond the optimal range, nanoparticle toxicity becomes dominant.

Table 3 : Summary of individual OFAT optimisation results and combined-condition biohydrogen production with and without silver nanoparticle (AgNP) supplementation

Experimental condition	Parameter tested	Cumulative biohydrogen production (mmol L^{-1})	Fold increase
Inoculum optimum	5 % (v/v)	14.52 ± 3.31	–
Growth-condition optimum	Light anaerobic	21.57 ± 3.66	–
Carbon-source optimum	Maltose	83.21 ± 1.34	–
Temperature optimum	40 °C	136.06 ± 5.20	–
Combined condition (control)	10 % + anaerobic light + maltose + 30 °C	194.86 ± 6.15	13.4× / 9.0× / 2.3× / 1.4×
+ AgNP 0.04 g L^{-1}	–	195.51 ± 5.62	1.00× (control)
+ AgNP 0.08 g L^{-1}	–	198.28 ± 3.68	1.02× (control)
+ AgNP 0.12 g L^{-1}	–	185.56 ± 6.99	0.95× (control)

Note: Fold increases for the combined condition are presented relative to the respective individual optimum values

The lack of statistical significance in the present study suggests that although AgNPs may improve electron transfer and metabolic efficiency, their overall impact remains limited under the tested conditions and is likely strain- and system-dependent. Collectively, these findings reinforce the concept that nanoparticle supplementation operates within a narrow optimal window, beyond which inhibitory effects outweigh potential benefits, underscoring the importance of precise dosage optimization in nanoparticle-assisted biohydrogen production systems. Growth analysis under nanoparticle supplementation further confirmed that AgNPs did not significantly affect bacterial growth dynamics, as OD profiles remained comparable across treatments.

4.0 CONCLUSION

Overall, this study demonstrates that biohydrogen production by locally isolated PNSB is governed by a complex interplay among microbial physiology, environmental conditions, and process optimization. Among the isolates, *Rhodopseudomonas palustris* PNSB_P exhibited superior performance, underscoring the importance of strain selection in biohydrogen research. The findings further emphasize that substrate type and redox conditions are the most critical determinants of hydrogen production, whereas factors such as inoculum size and moderate temperature variations play secondary roles. The limited but observable influence of AgNPs suggests potential for nanotechnology integration, although further optimization is required to achieve significant improvements.Collectively, this work provides valuable insights into optimizing the use of locally sourced

PNSB for sustainable biohydrogen production and contributes to the development of efficient, environmentally friendly bioenergy systems.

Acknowledgment

This study was supported by Universiti Teknologi Malaysia Grant 04K29. The authors would like to express their sincere gratitude to Universiti Teknologi Malaysia (UTM) for providing the opportunity and facilities to carry out this research. Special appreciation is extended to the Faculty of Science, Department of Biosciences, for their support, guidance, and access to laboratory resources throughout this study.

References

1. Abd-Alla, M. H., Bashandy, S. R., Sleem, W. A., & Khalaf, D. M. (2025). Sustainable biohydrogen production from banana peels using microbial fermentation. *BMC Biotechnology 2025 26:1*, *26*(1), 5-. https://doi.org/10.1186/s12896-025-01080-3
2. Abdul Aziz, A. H., Engliman, N. S., Mansor, M. F., Abdul, P. M., Arisht, S. N., Jamali, N. S., & Tiang, M. F. (2022). Synergistic enhancement of biohydrogen production by supplementing with green synthesized magnetic iron nanoparticles using thermophilic mixed bacteria culture. *International Journal of Hydrogen Energy*, *47*(96), 40683–40695. https://doi.org/10.1016/j.ijhydene.2022.09.105
3. Akpasi, S. O., Smarte Anekwe, I. M., Tetteh, E. K., Amune, U. O., Mustapha, S. I., & Kiambi, S. L. (2025). Hydrogen as a clean energy carrier: advancements, challenges, and its role in a sustainable energy future. *Clean Energy*, *9*(1), 52–88. https://doi.org/10.1093/ce/zkae112
4. Al-Mohammedawi, H. H., Znad, H., & Eroglu, E. (2018). Synergistic effects and optimization of photo-fermentative hydrogen production of Rhodobacter sphaeroides DSM 158. *International Journal of Hydrogen Energy*, *43*(33), 15823–15834. https://doi.org/10.1016/J.IJHYDENE.2018.06.140
5. Armbrecht, M. (2013). *Detection of contamination in DNA and protein samples by photometric measurements*.
6. Ashwini S Thakre, Diwakar Z Shende, & Kailas L Wasewar. (2024). Nanotechnology approaches for Enhancement in Biohydrogen Production. *Journal of Environmental Nanotechnology*, *13*(2), 277–293. https://doi.org/10.13074/jent.2024.06.242612
7. Asif, A., Mohsin, H., & Rehman, Y. (2021). Purple nonsulfur bacteria: An important versatile tool in biotechnology. In *Recent Advancement in Microbial Biotechnology* (pp. 309–337). Elsevier. https://doi.org/10.1016/B978-0-12-822098-6.00003-3
8. Bartoš, O., Chmel, M., & Swierczková, I. (2024). The overlooked evolutionary dynamics of 16S rRNA revises its role as the “gold standard” for bacterial species identification. *Scientific Reports 2024 14:1*, *14*(1), 9067-. https://doi.org/10.1038/s41598-024-59667-3
9. Bayon-Vicente, G., Toubeau, L., Gilson, M., Gégo, G., Landgey, N., Krings, S., & Leroy, B. (2025). Metabolic pathways to sustainability: review of purple non-sulfur bacteria potential in agri-food waste valorization. *Frontiers in Bioengineering and Biotechnology*, *13*, 1529032. https://doi.org/10.3389/fbioe.2025.1529032
10. Bianchi, L., Mannelli, F., Viti, C., Adessi, A., & De Philippis, R. (2010). Hydrogen-producing purple non-sulfur bacteria isolated from the trophic lake Averno (Naples, Italy). *International Journal of Hydrogen Energy*, *35*(22), 12216–12223. https://doi.org/10.1016/J.IJHYDENE.2010.08.038
11. Bosman, C. E., Pott, R. W. M. C., & Bradshaw, S. M. (2023). The effect of light emission spectrum on biohydrogen production by Rhodopseudomonas palustris. *Bioprocess and Biosystems Engineering 2023 46:6*, *46*(6), 913–919. https://doi.org/10.1007/S00449-023-02863-8
12. Cha, M., Park, M. S., & Kim, S. J. (2025). Biological Routes for Biohydrogen Production: A Clean and Carbon-Free Fuel. *Biotechnology Journal*, *20*(7), e70074. https://doi.org/10.1002/BIOT.70074
13. Choe, H. W., Kim, D. A., Choi, Y. J., Koh, H. G., & Park, W. K. (2025a). Influence of Microalgal Cell Division Tendency on OD to DCW Conversion Factor and Chlorophyll Contents. *Journal of Microbiology and Biotechnology*, *35*, e2412049. https://doi.org/10.4014/JMB.2412.12049
14. Choe, H. W., Kim, D. A., Choi, Y. J., Koh, H. G., & Park, W. K. (2025b). Influence of Microalgal Cell Division Tendency on OD to DCW Conversion Factor and Chlorophyll Contents. *Journal of Microbiology and Biotechnology*, *35*, e2412049. https://doi.org/10.4014/JMB.2412.12049
15. de Souza, P. A., Ramos, J. N., Vasconcellos, L., Costa, L. V., Forsythe, S. J., & Brandão, M. L. L. (2025). Application and Limitations of 16S rRNA Gene Sequencing for Identifying WHO Priority Pathogenic Gram-Negative Bacilli. *Infection and Drug Resistance*, *18*, 6353. https://doi.org/10.2147/IDR.S550704

16. Dhar, K., Venkateswarlu, K., & Megharaj, M. (2023). Anoxygenic phototrophic purple non-sulfur bacteria: tool for bioremediation of hazardous environmental pollutants. *World Journal of Microbiology & Biotechnology*, *39*(10), 283. https://doi.org/10.1007/S11274-023-03729-7
17. Dogmaz, S., & Cavas, L. (2023). Biohydrogen production via green silver nanoparticles synthesized through biomass of Ulva lactuca bloom. *Bioresource Technology*, *379*, 129028. https://doi.org/10.1016/j.biortech.2023.129028
18. du Toit, J. P., & Pott, R. W. M. (2021). Heat-acclimatised strains of Rhodopseudomonas palustris reveal higher temperature optima with concomitantly enhanced biohydrogen production rates. *International Journal of Hydrogen Energy*, *46*(21), 11564–11572. https://doi.org/10.1016/J.IJHYDENE.2021.01.068
19. Elazab, M. A., Elgohr, A. T., Bassyouni, M., Kabeel, A. E., Attia, M. E. H., Elshaarawy, M. K., Hamed, A. K., & Alzahrani, H. A. H. (2025). Green Hydrogen: Unleashing the Potential for Sustainable Energy Generation. *Results in Engineering*, *27*(2), 106031. https://doi.org/10.1016/j.rineng.2025.106031
20. Gokfiliz-Yildiz, P., & Karapinar, I. (2018). Optimization of particle number, substrate concentration and temperature of batch immobilized reactor system for biohydrogen production by dark fermentation. *International Journal of Hydrogen Energy*, *43*(23), 10655–10665. https://doi.org/10.1016/J.IJHYDENE.2018.01.036
21. Gupta, S., Fernandes, A., Lopes, A., Grasa, L., & Salafranca, J. (2024). Photo-Fermentative Bacteria Used for Hydrogen Production. *Applied Sciences 2024, Vol. 14, 14*(3). https://doi.org/10.3390/app14031191
22. Hackmann, T. J. (2025). Setting new boundaries of 16S rRNA gene identity for prokaryotic taxonomy. *International Journal of Systematic and Evolutionary Microbiology*, *75*(4), 006747. https://doi.org/10.1099/IJSEM.0.006747
23. Hellal, M. S., Gamon, F., Cema, G., Hassan, G. K., Mohamed, G. G., & Ziembińska-Buczyńska, A. (2024). Nanoparticle-assisted biohydrogen production from pretreated food industry wastewater sludge: Microbial community shifts in batch and continuous processes. *Energy Conversion and Management*, *299*. https://doi.org/10.1016/j.enconman.2023.117824
24. Hu, C., Choy, S. Y., & Giannis, A. (2018). Evaluation of Lighting Systems, Carbon Sources, and Bacteria Cultures on Photofermentative Hydrogen Production. *Applied Biochemistry and Biotechnology*, *185*(1), 257–269. https://doi.org/10.1007/s12010-017-2655-5
25. Huang, P., & Zhou, Y. (2026). Metabolic responses of purple phototrophic bacteria to elevated hydrogen partial pressure: Metatranscriptomic insights into biohydrogen production and consumption. *Bioresource Technology*, *443*, 133831. https://doi.org/10.1016/J.BIORTECH.2025.133831
26. Iwuji, C., Saha, H., Ghann, W., Dotson, D., Bhuiya, Md. A. K., Parvez, Md. S., Jahangir, Z. S., Rahman, M. M., Chowdhury, F. I., & Uddin, J. (2024). Synthesis and characterization of silver nanoparticles and their promising antimicrobial effects. *Chemical Physics Impact*, *9*, 100758. https://doi.org/10.1016/j.chphi.2024.100758
27. Jiang K, Bai R, Gao T, Lu P, Zhang J, Zhang S, Xu F, Wang S, Zhao H. Optimization of hydrogen production in Enterobacter aerogenes by Complex I peripheral fragments destruction and maeA overexpression. Microb Cell Fact. 2023 Jul 26;22(1):137. doi: 10.1186/s12934-023-02155-6. PMID: 37496040; PMCID: PMC10373349.
28. Kharisma, A. D., Amekan, Y., Sarto, & Cahyanto, M. N. (2022). Effect of Hydrogen Peroxide on Hydrogen Production from Melon Fruit (Cucumis melo L.) Waste by Anaerobic Digestion Microbial Community. *International Journal of Renewable Energy Development*, *11*(1), 95–101. https://doi.org/10.14710/IJRED.2022.40883
29. Laurinavichene, T., & Tsygankov, A. (2018). Inoculum density and buffer capacity are crucial for H2 photoproduction from acetate by purple bacteria. *International Journal of Hydrogen Energy*, *43*(41), 18873–18882. https://doi.org/10.1016/J.IJHYDENE.2018.08.095
30. Lo, S. C., Shih, S. H., Chang, J. J., Wang, C. Y., & Huang, C. C. (2012). Enhancement of photoheterotrophic biohydrogen production at elevated temperatures by the expression of a thermophilic clostridial hydrogenase. *Applied Microbiology and Biotechnology*, *95*(4), 969–977. https://doi.org/10.1007/S00253-012-4017-0
31. Lucena-Aguilar, G., Sánchez-López, A. M., Barberán-Aceituno, C., Carrillo-Ávila, J. A., López-Guerrero, J. A., & Aguilar-Quesada, R. (2016). DNA Source Selection for Downstream Applications Based on DNA Quality Indicators Analysis. *Biopreservation and Biobanking*, *14*(4), 264. https://doi.org/10.1089/BIO.2015.0064
32. Martínez, M. E., Jorquera, L., Poirrier, P., Díaz, K., & Chamy, R. (2023). Effect of Inoculum Size and Age, and Sucrose Concentration on Cell Growth to Promote Metabolites Production in Cultured Taraxacum officinale (Weber) Cells. *Plants*, *12*(5), 1116. https://doi.org/10.3390/PLANTS12051116/S1
33. Maturi, K. C., Madeti, S. R. K., Sinha, S., Saikia, S., Srivastava, A., & Haq, I. (2026). Revolutionizing bio-hydrogen production: smart integration of nanotechnology, microbial engineering, and circular waste valorisation. *Bioresources and Bioprocessing*, *13*(1), 17. https://doi.org/10.1186/s40643-025-01001-4
34. McKinlay, J. B. (2014). *Systems Biology of Photobiological Hydrogen Production by Purple Non-sulfur Bacteria* (pp. 155–176). https://doi.org/10.1007/978-94-017-8554-9_7
35. Mohr, T., Aliyu, H., Biebinger, L., Gödert, R., Hornberger, A., Cowan, D., de Maayer, P., & Neumann, A. (2019). Effects of different operating parameters on hydrogen production by Parageobacillus thermoglucosidasius DSM 6285. *AMB Express*, *9*(1), 207. https://doi.org/10.1186/S13568-019-0931-1

36. Mona, S., Kumar, S. S., Kumar, V., Parveen, K., Saini, N., Deepak, B., & Pugazhendhi, A. (2024). Optimization and enhancement of biohydrogen production in a single-stage hybrid (dark/photo) fermentation reactor using Fe3O4 and TiO2 nanoparticles. *International Journal of Hydrogen Energy*, *52*, 295–305. https://doi.org/10.1016/j.scitotenv.2020.138481
37. Monir, M. U., Aziz, A. A., Ahmed, M. T., & Hasan, M. Y. (2022). Hydrogen energy–Potential in developing countries. *Renewable Energy and Sustainability: Prospects in the Developing Economies*, 299–325. https://doi.org/10.1016/B978-0-323-88668-0.00013-9
38. Morrison, H. M., & Bose, A. (2024). Purple non-sulfur bacteria for biotechnological applications. *Journal of Industrial Microbiology & Biotechnology*, *52*, kuae052. https://doi.org/10.1093/JIMB/KUAE052
39. Navid, A., Jiao, Y., Wong, S. E., & Pett-Ridge, J. (2019). System-level analysis of metabolic trade-offs during anaerobic photoheterotrophic growth in Rhodopseudomonas palustris. *BMC Bioinformatics 2019 20:1*, *20*(1), 233-. https://doi.org/10.1186/S12859-019-2844-Z
40. Posada, D., & Crandall, K. A. (2021). Felsenstein Phylogenetic Likelihood. *Journal of Molecular Evolution*, *89*(3), 134. https://doi.org/10.1007/S00239-020-09982-W
41. Ramin, K. I., & Allison, S. D. (2019). Bacterial Tradeoffs in Growth Rate and Extracellular Enzymes. *Frontiers in Microbiology*, *10*, 494333. https://doi.org/10.3389/FMICB.2019.02956/TEXT
42. Rashid, N., Onwusogh, U., & Mackey, H. R. (2022). Exploring the metabolic features of purple non-sulfur bacteria for waste carbon utilization and single-cell protein synthesis. *Biomass Conversion and Biorefinery 2022 14:12*, *14*(12), 12653–12672. https://doi.org/10.1007/S13399-022-03273-8
43. Russo, P., Lancia, M. C., Lauri, R., Gottardo, M., & Valentino, F. (2026). Biohydrogen production from biowaste: Assessment of the flammability of bioreactors gaseous mixtures. *Journal of Loss Prevention in the Process Industries*, *102*(13), 105994. https://doi.org/10.1016/j.jlp.2026.105994
44. Sagir, E., Ozgur, E., Gunduz, U., Eroglu, I., & Yucel, M. (2017). Single-stage photofermentative biohydrogen production from sugar beet molasses by different purple non-sulfur bacteria. *Bioprocess and Biosystems Engineering*, *40*(11), 1589–1601. https://doi.org/10.1007/s00449-017-1815-x
45. Sakarika, M., Spanoghe, J., Sui, Y., Wambacq, E., Grunert, O., Haesaert, G., Spiller, M., & Vlaeminck, S. E. (2019). Purple non-sulphur bacteria and plant production: benefits for fertilization, stress resistance and the environment. *Microbial Biotechnology*, *13*(5), 1336. https://doi.org/10.1111/1751-7915.13474
46. Sakarika, M., Spanoghe, J., Sui, Y., Wambacq, E., Grunert, O., Haesaert, G., Spiller, M., & Vlaeminck, S. E. (2020). Purple non-sulphur bacteria and plant production: benefits for fertilization, stress resistance and the environment. *Microbial Biotechnology*, *13*(5), 1336–1365. https://doi.org/10.1111/1751-7915.13474
47. Singla, S., Jana, A., Thakur, R., Kumari, C., Goyal, S., & Pradhan, J. (2022). Green synthesis of silver nanoparticles using Oxalis griffithii extract and assessing their antimicrobial activity. *OpenNano*, *7*, 100047. https://doi.org/10.1016/j.onano.2022.100047
48. Stal, L. J. (2017). The effect of oxygen concentration and temperature on nitrogenase activity in the heterocystous cyanobacterium Fischerella sp. *Scientific Reports*, *7*(1), 5402. https://doi.org/10.1038/S41598-017-05715-0
49. Tiang, M. F., Hanipa, M. A. F., Mahmod, S. S., Zainuddin, M. T., Lutfi, A. A. I., Jahim, J. M., Takriff, M. S., Reungsang, A., Wu, S. Y., & Abdul, P. M. (2024). Impact of light spectra on photo-fermentative biohydrogen production by Rhodobacter sphaeroides KKU-PS1. *Bioresource Technology*, *394*, 130222. https://doi.org/10.1016/J.BIORTECH.2023.130222
50. Tripathi, N., Zubair, M., & Sapra, A. (2025). Gram Staining. *StatPearls [Internet]*. https://www.ncbi.nlm.nih.gov/books/NBK562156/
51. Ulhiza, T. A., Puad, N. I. M., & Azmi, A. S. (2022). Statistical Screening of Physico-Chemical Factors for Biohydrogen. *Journal of Engineering Science and Technology*, *17*(5), 3012–3024.
52. Wang, M., Liu, S., Wang, Z., Li, B., Li, L., Wang, Z., Zhou, G., & Sui, Z. (2022). Accurate and online quantification of viable *Rhodobacter sphaeroides* cells using a flow cytometry-dielectric spectroscopy (FCM-DS) method. *Talanta*, *245*, 123448. https://doi.org/10.1016/J.TALANTA.2022.123448
53. Webster, G., Blazejak, A., Cragg, B.A., Schippers, A., Sass, H., Rinna, J., Tang, X., Mathes, F., Ferdelman, T.G., Fry, J.C., Weightman, A.J. and Parkes, R.J. (2009), Subsurface microbiology and biogeochemistry of a deep, cold-water carbonate mound from the Porcupine Seabight (IODP Expedition 307). Environmental Microbiology, 11: 239-257. https://doi.org/10.1111/j.1462-2920.2008.01759.x
54. Wu, X., Wang, X., Yang, H., & Guo, L. (2010). A comparison of hydrogen production among three photosynthetic bacterial strains. *International Journal of Hydrogen Energy*, *35*(13), 7194–7199. https://doi.org/10.1016/J.IJHYDENE.2009.12.141
55. Yildirim, O., & Ozkaya, · Bestami. (2025). *Enhancing fermentation yield for biohydrogen production using eco-friendly nickel and cobalt ferrite nanoparticles*. *15*, 26613–26622. https://doi.org/10.1007/s13399-024-05354-2

56. Yildirim, O., Tunay, D., Ozkaya, B., & Demir, A. (2022). Effect of Green synthesized silver oxide nanoparticle on biological hydrogen production. *International Journal of Hydrogen Energy*, *47*(45), 19517–19525. https://doi.org/10.1016/j.ijhydene.2021.11.176
57. Zhang, J., Xue, D., Wang, C., Fang, D., Cao, L., & Gong, C. (2023). Genetic engineering for biohydrogen production from microalgae. *IScience*, *26*(8), 107255. https://doi.org/10.1016/j.isci.2023.107255